Modelling and characterisation of piezoelectrically actuated bistable composites

C.R.Bowen[1], P.F.Giddings[1], A.I.T Salo[2] and H.A.Kim[1]

[1] Materials Research Centre, Department of Mechanical Engineering, University of Bath, Bath, BA2 7AY, UK.

[2] Sport and Exercise Science, University of Bath, Bath, BA2 7AY, UK.

Abstract

This paper aims to develop and validate an ANSYS finite element model to predict both the cured shape and snap-through of unsymmetric bistable laminates actuated by piezoelectric macro fibre composites attached to the laminate. To fully describe piezoelectric actuation the three dimensional compliance $[s_{ij}]$, piezoelectric $[d_{ij}]$ and relative permittivity $[\varepsilon_{ij}]$ matrices were formulated for the macro fibre actuator. The deflection of an actuated isotropic aluminium beam was then modelled and compared to experimental measurements to validate the data. The model was then extended to bistable laminates actuated using macro fibre composites. Model results were compared to experimental measurements of laminate profile (shape) and snap-through voltage. The modelling approach is an important intermediate step toward enabling design of shape-changing structures based on bistable laminates.

I. Introduction

For aerospace applications the use of morphing surfaces and smart materials can reduce drag [1], provide load alleviation and enable aerodynamic control [2]. Unsymmetric bistable laminates have been proposed as a materials solution for morphing and shape changing components [3,4]. Bistable composites can maintain two significantly different shapes without a continuous energy input, requiring only actuation to initiate a transition between states. Piezoelectric materials, such a Macro Fibre Composites (MFCs) [3], have been used to induce 'snap-through' bistable composites from one stable state to another. Fig. 1 shows the two stable states, 'State-A' and 'State-B', of a bistable carbon fibre reinforced plastic (CFRP) combined with a piezoelectric MFC. The CFRP is an unsymmetric $[0/90]_T$ laminate where an anisotropy of the coefficient of thermal expansion leads to a residual stress on cooling from the cure temperature and induces a curvature and the existence two stable equilibrium states.

The cured shape and snap-through behaviour of bistable laminates without integrated piezoelectric materials has been investigated with analytical [5] and finite element techniques [6]. Attempts to predict piezoelectric-induced 'snap-through' of a combined CFRP-MFC composite from one stable state to

another has proven more challenging due to the multi-physics nature of the problem. This paper presents a homogenised coupled multi-physics model of MFC based piezoelectric actuation and integrates it with a bistable CFRP laminate model. After an initial review of existing work to date on bistable composite and piezoelectric actuation (Section II), the paper will develop the compliance [s^T_{ij}], piezoelectric [d_{ij}] and relative permittivity [ε^T_{ij}] matrices of the MFC (Section III). The approach is then validated by modelling a simple isotropic beam under open and closed circuit conditions (Section IV). Finally, the model will be extended to include an MFC attached to a bistable laminate (Section V). Both the cured shape and snap-through actuation of the piezoelectrically actuated CFRP-MFC combination will be modelled and compared to experimental measurements.

II. Background

A. MFC Construction

The actuators used were from Smart Materials GmbH (Dresden, Germany) and consist of polycrystalline piezoelectric ceramic rods. Copper interdigitated electrodes are attached to the upper and lower surfaces to apply an electric field parallel to the rod length. The piezoelectric ceramic is a lead zirconate titanate material (PZT), in this case PZT-5A since this is a 'soft' PZT which exhibits high piezoelectric d_{33} and d_{31} coefficients, i.e. a high strain per unit electric field [7]. To maximise the strain per unit electric field, the poling direction of the PZT is aligned along the rod length using the interdigitated electrodes. This ensures that the actuation strain is generated via the d_{33} coefficient, which is typically twice the d_{31} coefficient [8, 9]. The electrode arrangement also improves damage tolerance; since the electric field is applied at regular intervals along the rod length and any damage/ fracture of the rod or electrode merely reduces the functionality of a small region surrounding the defect and does not significantly reduce global actuator performance [9].

B. MFC modelling approaches and bistable actuation

Efforts to model the microscopic behaviour of the constituent materials of the MFC are ongoing with several workers using both finite element [10, 11] and analytical techniques [12-14]. While these efforts bring insight into the underlying mechanisms of MFC function and provide tools to aid in actuator design (optimising electrode placement and fibre/rod shape etc.) the level of complexity in this micromechanical modelling is too computationally expensive for integration within a larger macro-scale structural model, such as a bistable laminate. Despite interest in MFC actuators for use in structural actuation schemes, [16-18] little work adequately captures the change in actuator response with electrical boundary conditions during actuation of bistable laminates. Several investigators [16, 18] have chosen to approximate the

piezoelectric strain by altering the coefficient of thermal expansion of the macro fibre composite model to create actuation strains. While such research efforts provide approximations to actuator behaviour, in order to achieve accurate representation of the electromechanical coupling inherent in piezoelectric devices the elastic and electrical conditions within a device must be coupled. In addition, thermal approximations would not allow design of combined control and actuation systems utilising MFC sensor capabilities, which requires prediction of voltage generated within the MFC in response to applied stress. To highlight this, equation 1 shows the relationship between the closed circuit or constant field compliance (s_{ij}^{E}) and open circuit or constant electric displacement compliance (s_{ij}^{D}) [19]. These two quantities are related via the square of the electromechanical coupling coefficient (k^2), defined as the ratio of stored electrical energy to supplied mechanical energy.

$$1-k^2 = s_{ij}^{D} \Big/ s_{ij}^{E} \qquad \text{(Eqn. 1)}$$

As k^2 is always positive and less than unity, the closed circuit compliance is greater than the open circuit compliance. Based on a typical value for piezoelectric coupling coefficient k for PZT-5A of ~0.7 [20], the open circuit stiffness of the MFC is approximately twice the closed circuit stiffness.

To integrate the MFC model with a structural FE model, coupled-field finite elements that provide electromechanical coupling should be used. While MFCs has received attention as structural actuators [15, 21], less work has investigated their suitability for inducing snap-through in bistable laminates. Analytical techniques based on the Rayleigh-Ritz minimisation techniques of Hyer [5] have met with some success for the prediction of snap-through for MFC actuated bistable laminates [16, 18, 22]. Analytically predicted values for snap-through voltage often do not agree with experimental measurements, although the reduced computational cost has allowed investigators to conduct parametric studies relating to moisture absorption [23] and laminate architecture [24]. If bistable mechanisms are to be viable within morphing structures, they must be integrated within host structures and are subject to elastic boundary conditions imposed by the stiffness of the host. Current analytical models based on Hyer's energy minimisation method are not able to predict the cured shapes of bistable composite laminates embedded within host structures. Gude and Hufenbach [25] created a simple homogenised MFC model and investigated the use of MFCs to induce snap-through in bistable laminates. Analytical and finite element models were presented to model MFC device behaviour but no validation of the MFC model was presented and no comparison of FE-predicted snap-through voltage was made to experimental data. Dano et al. [21] presented a finite element analysis of MFCs used to compensate for thermal deformation of unsymmetric composite laminates. The actuation performance of the MFC model was validated against experimental measurement of the deflection of an aluminium beam and unidirectional

carbon/epoxy plates. Finite element predictions of beam deflection were in good agreement with experimental data, however no quantitative comparison of prediction error was presented. Recently, Binette et al. [17] conducted experimental characterisation of laminate deflection for a composite panel subjected to thermal loading. Piezoelectric actuation via two MFC actuators was used to reverse the induced thermal deformation. This experimental work was conducted to validate a coupled field finite element model of an unsymmetric laminate under combined piezoelectric and thermal actuation. The coupled field MFC model was based on Dano et al. [21] and shared the same set of material properties to represent the MFC. System behaviour under isothermal piezoelectric actuation and combined thermal-piezo loading was predicted using the FE model developed. In the case of combined thermal and piezoelectric loading prediction, accuracy varies between 4% and 31%.

Following an attempt to model bistable composite laminates using the commercial ANSYS FEA software (release V5.5.2), Gude and Hufenbach [25] attempted to model the snap-through of a bistable composite laminate using 8-node layered solid elements (SOLID46) to represent the laminate and 8-node coupled field brick elements (SOLID5) for the MFC. The $[0/90]_T$ laminate was manufactured from an unidentified pre-preg material using T300 carbon fibre reinforcement and measured 150×150×0.5mm. A Smart Materials MFC-8557P1 actuator was bonded to its upper surface. The element types used for both bistable composite and MFC volumes were linear solid elements [25]. Both element types approximate the displacement field between nodes using linear interpolation. This first order approximation to displacement introduces numerical errors in the analysis of highly curved structures [26]. As no details of mesh density were given in the work, it is not possible to determine if element size was reduced to minimise these errors. Furthermore the SOLID46 element is unsuitable for modelling curved structures. When the SOLID46 element is deformed, as occurs in highly curved bistable laminates, the element stiffness matrix is formulated assuming the element coordinate system remains parallel to the original coordinate system of the undeformed element [26]. No predicted snap-through voltage was presented and no comparison between the FE solution and either experimental data or analytical predictions was made. The authors simply state that snap-through was predicted. It should be noted that the analytical model presented by Gude et al. [25] in addition to the finite element model did not agree well with experimental data contained within the work. Analytically predicted values for snap-through voltage deviated from those observed in experiment by 130% (1260V predicted against 526V observed). Gude et al. [27] very recently presented a highly novel semi-analytical, geometrically non-linear simulation model using the Rayleigh-Ritz method with good agreement with experiments (snap through voltage). ANSYS finite element analysis was also examined by the authors and it was concluded that meshing the laminate and actuator with shell elements and simulating the piezoelectric strain of the MFC by thermal expansion was more appropriate for fast solution times.

Portela *et al.* [16] presented an analytical technique and a finite element model (FE) using ABAQUS/EXPLICIT to predict snap-through voltage for an MFC-actuated bistable laminate. The FE model approximated the behaviour of the MFC by applying a different thermal load to the MFC elements compared to the bistable composite elements. By scaling the coefficient of thermal expansion of the MFC elements to match the strain per unit electric field value of the MFC (d_{33}) a correlation between temperature change within the MFC elements and drive voltage was obtained. In addition, Portela *et al.* [16] predicted the effect of moisture on laminate curvature and snap-through voltage for a range of materials and actuator sizes. They suggested that for any given laminate there is an optimum size of actuator which is capable of initiating snap-through without significantly impacting on the cured shape of the composite laminate. This was supported by the FE analyses, though the work did not contain validating experimental data. Only a single experimental measurement of snap-through voltage is presented by Portela *et al.* [16] with no explanation of which particular laminate was tested to achieve the observed snap-through of 390V. Without laminate descriptions, test conditions or experimental procedures being clarified it was not possible to determine the extent to which the presented model agrees with experimental data. However, the insights gained into possible effects of moisture absorption on bistable laminates and their snap-through behaviour are valuable contributions to the field.

Currently no adequate finite element model exists to predict the actuation behaviour of MFC actuated bistable laminates, and therefore this paper describes the formulation and validation of a coupled field finite element model to predict both snap-through voltage and cured shape of MFC actuated bistable laminates using the commercial FE-software ANSYS V11.0. We aim to compare model predictions with detailed experimental characterisation.

III. MFC Model Formulation and validation

A. Compliance matrix [s^{E}_{ij}] formulation

The three dimensional compliance matrix of the MFC was populated by converting the four linear elastic engineering constants measured by Williams *et al.* [28] in Table 1 into equation 2. This equation was derived from the standard stress-strain relations for orthotropic materials presented in [29]. The resulting compliance matrix is of the standard form for a transversely isotropic material with a single axis of rotational symmetry parallel with the poling direction in PZT fibres.

$$\left[s_{ij}^{E}\right]=\begin{bmatrix} 1/E_1 & -\nu_{31}/E_1 & -\nu_{31}/E_3 & 0 & 0 & 0 \\ -\nu_{31}/E_1 & 1/E_1 & -\nu_{31}/E_3 & 0 & 0 & 0 \\ -\nu_{31}/E_3 & -\nu_{31}/E_3 & 1/E_3 & 0 & 0 & 0 \\ 0 & 0 & 0 & 1/G_{31} & 0 & 0 \\ 0 & 0 & 0 & 0 & 2(1+\nu_{31})/E_3 & 0 \\ 0 & 0 & 0 & 0 & 0 & 2(1+\nu_{31})/E_3 \end{bmatrix} \quad \text{(Eqn. 2)}$$

where E is the Young's modulus, G is the shear modulus, v is the Poisson's ratio of the material and the subscripts denote the orientation of each property with respect to the material coordinate system (the 3-direction is the poling direction). For comparison, the manufacturers (Smart Materials GmbH, Dresden) data sheet values [30] are also presented in Table 1 and are in good agreement with measured values presented in [28]. The final s^{E}_{ij} matrix used to define the compliance of the MFC model is shown in equation 3.

$$\left[s_{ij}^{E}\right]=\begin{bmatrix} 0.065 & -0.0205 & -0.0106 & 0 & 0 & 0 \\ -0.0205 & 0.065 & -0.0106 & 0 & 0 & 0 \\ -0.0106 & -0.0106 & 0.034 & 0 & 0 & 0 \\ 0 & 0 & 0 & 0.165 & 0 & 0 \\ 0 & 0 & 0 & 0 & 0.173 & 0 \\ 0 & 0 & 0 & 0 & 0 & 0.173 \end{bmatrix} \times 10^{-9} m^2 N^{-1} \quad \text{(Eqn. 3)}$$

B. Piezoelectric matrix [d_{ij}] formulation

The effective piezoelectric constants for the device were determined in order to describe the response of the MFC to an applied electric field. As described by [9, 10], the relationships between the piezoelectric properties of the constituent materials and the complete MFC are highly complex due to non-uniform polarisation of PZT fibres and the composite structure of the actuator. While predictive models for free-strain behaviour agree well with experiment [9, 14], experimental measurement of device behaviour provides the best available data on which to base the FE model for this work. Williams *et al.* [9] experimentally determined the free-strain behaviour of the same MFC actuator used in the present study (Smart Materials Corp M8557-P1). The value for d_{33} (strain per unit electric field in poling direction) presented in [9] agrees with data presented by the manufacturer [30], however no value for d_{31} was

reported by either source. Williams *et al.* determined d_{33} and d_{31} for an 'Active Fibre Composite' [9] and the construction and mode of operation is sufficiently similar to an MFC to assume that the measured ratio of d_{31}/d_{33} to be equal in both devices [28]. The values for both d_{31} and d_{32} shown in Table 2 were calculated by multiplying the measured piezoelectric d_{33} constant taken from Smart Materials product specification [30] by the d_{31}/d_{33} ratio of -0.449 measured by Williams *et al* [9]. The calculated values used to populate the piezoelectric coefficient [d_{ij}] matrix used in the present FE-model of the MFC are shown in Table 2 and the final matrix is shown in equation 4. No shear piezoelectric coefficients are included in the matrix (e.g. d_{15}). For conventional piezoelectric ceramics d_{15} is non-zero, however in many composites $|d_{15}|<<|d_{3j}|$. In addition, since the applied electric field will always be along the poling direction (fibre/rod axis) no contribution for the piezoelectric shear coefficients are expected.

$$\left[d_{ij}\right]=\begin{bmatrix} -2.1 & -2.1 & 4.67 & 0 & 0 & 0 \\ 0 & 0 & 0 & 0 & 0 & 0 \\ 0 & 0 & 0 & 0 & 0 & 0 \end{bmatrix}\times 10^{-10}\ pmV^{-1} \qquad \text{(Eqn. 4)}$$

C. Relative permittivity matrix formulation

To fully specify the electromechanical coupling within the MFC the relative permittivity of the active layer must be determined. This property is important in providing the relationship between charge Q [C], capacitance C [F] and voltage (V) for the MFC ($Q = CV$), and determines the magnitude of the induced electric field when subjected to a mechanical stress under open circuit conditions. To determine the relative permittivity of the active layer a micromechanical mixing rule for ε^{T}_{33} presented by Deraemaeker [13] was used along with a standard mixing rule for dielectric volumes in series representing ε^{T}_{22} [13]; namely equations 5 and 6.

$$\varepsilon^{T}_{33} = \rho\varepsilon^{T,p}_{33} + (1-\rho)\varepsilon^{T,m}_{33} \qquad \text{(Eqn. 5)}$$

$$\frac{1}{\varepsilon^{T}_{22}} = \left(\rho\varepsilon^{T,p}_{22}\right)\left(\frac{(1-\rho)\varepsilon^{T,m}_{22}}{\rho\varepsilon^{T,p}_{22} + (1-\rho)\varepsilon^{T,m}_{22}}\right) \qquad \text{(Eqn. 6)}$$

where ε^{T}_{ij} is the relative permittivity and ρ the volume fraction of PZT within the active layer. The superscripts m and p denote the piezoelectric and matrix materials respectively. The relative permittivity of PZT-5A data used to calculate the permittivity of the MFC device was taken from Jaffe [20] with the value for the epoxy matrix taken from Deraemaeker [13]. The wide variation in the predicted relative permittivity values between the ε^{T}_{11} and ε^{T}_{22} is due to the different electrical conditions in the *1* and *2*-

directions. For an electric field to propagate in the *2*-direction it must permeate through the epoxy layer and the PZT fibre. This means that the low permittivity of the epoxy significantly reduces the effective permittivity of the active layer in this direction.

IV. MFC validation on isotropic beam

To validate the homogenised materials properties describing the MFC actuator, it was necessary to compare FE model predictions of actuator deflection with experimental data. Two MFC actuators were bonded to a simple aluminium cantilever with acting as an actuator and the second remaining passive to allow testing of the influence of electrical boundary conditions.

A. Experimental setup

Two MFC actuators (Smart Materials Corp M-8557P1) were bonded to the front and back surfaces of an aluminium beam measuring 330×75×1.97 mm as in Fig. 2. The actuators and aluminium surfaces were cleaned using isopropyl alcohol and a thin coat of a two-part epoxy adhesive applied to both surfaces. The MFCs were then carefully located whilst ensuring no air-bubbles were trapped during placement. With the MFCs in place, the assembly was placed under 200N clamping force for 24hrs to allow the epoxy to cure. Both MFCs (labelled MFC-1 and MFC-2 in Fig. 2) were positioned so that the active area was positioned between z = 45 mm and z = 130 mm, with the poling direction of the PZT fibres (*3*-direction) parallel with the z-axis. The beam was clamped so that the 75 mm dimension (x-direction) was aligned vertically. This arrangement isolated beam deflection (D_y) from the influence of gravitational forces. A Nippon LAS5010v laser displacement sensor with a resolution of 10 μm was used to measure cantilever deflection as a function of applied voltage. The active MFC (MFC-1) was driven from a signal generator attached to a Trek PZD700 Piezodriver. Closed circuit boundary conditions were imposed on MFC-2 by connecting the positive and earth electrode terminals, while for open circuit conditions these terminals were insulated from one another. Piezoelectric actuators are subject to slow creep under open loop control [31] due to domain motion. To standardise the piezoelectric creep effects [32], all measurements at each voltage were taken after a 60 second settling period. Beam deflection at z = 120 mm as a function of MFC-1 drive voltage was measured from 0 – 400V taken at 80V intervals. Deflection measurements were carried out with MFC-2 under closed circuit boundary conditions. A datum measurement of beam position was taken before voltage application and this value subtracted from the actuated beam position to calculate the deflection.

To measure the change in beam deflection due to changing electric boundary conditions of MFC-2 beam deflection in response to 400V MFC-1 drive voltage was measured at intervals of 30 mm between z = 120

mm and z = 300 mm. Closed and open circuit measurements were taken sequentially at each z = position. A separate datum measurement was taken for each measurement and both MFC-1 and MFC-2 were electrically discharged between measurements.

B. FEM model of MFC actuated isotropic beam

The aluminium cantilever was modelled using 20-node quadratic brick SOLID186 elements with isotropic mechanical properties (Young's modulus 70.7GPa and Possion's ratio 0.32). The two MFC actuators were represented by 20-node quadratic brick SOLID226 elements. SOLID226 elements are coupled field elements which solve the constitutive equations for an elastic piezoelectric solid. In addition to the improved solution accuracy of the 20-node quadratic elements in modelling highly curved structures, when combining element types within a single model it is advisable to use 20-node elements throughout [33] to ensure that all nodes on adjacent elements are coincident. Attempting to merge nodes linked to a volume meshed with 8-node elements with 20-node elements connected with an adjacent volume can result in nodes losing connectivity with the model, introducing numerical errors and preventing model solution. Once the model was appropriately meshed, the model consisted of a total of 4680 SOLID186 elements for beam and 340 SOLID226 elements within the MFC volume. Element density was sufficient to accurately capture beam behaviour as further refinement of the mesh did not significantly affect the predicted beam deflection.

The MFC model volumes were positioned on the front and back surfaces of the cantilever as in Fig. 2 with all coincident nodes on the contact surfaces merged to ensure stress transfer between cantilever and actuator volumes. The clamped mechanical boundary condition was modelled by constraining all three translational degrees of freedom (x, y,& z) for nodes lying in the range -30 mm < x < 0 mm on the y = 0 mm plane. Nodes in the same range of x-coordinate on the y = 0.197 mm plane were constrained in the y-direction only. The finite element model used to predict deflection of the experimental beam in response to MFC actuation is shown in Fig. 3. In creating the piezoelectric $[d_{ij}]$ and permittivity $[\varepsilon_{ij}]$ matrices for the MFC actuator it is assumed that electric field is constant along and aligned with the z-axis. To ensure a constant and well aligned electric field, the voltage degree of freedom for nodes of equal z-coordinate was coupled to create planes of equal voltage at 5 mm intervals along the z-direction of the MFC volume. To model MFC behaviour under closed circuit boundary conditions (i.e. two electrodes of MFC-2 are electrically connected) the induced potential difference as a result of a stress must be dissipated; however it is inappropriate to constrain all voltage DOFs within the MFC volume as it reduces solution accuracy [33]. Furthermore, simply altering the voltage constraints at the x = 35 mm and x = 120 mm faces would not suppress the induced field throughout the volume but only near the extremities. To suppress the

induced field throughout the passive MFC volume (MFC-2 in Fig. 2) the piezoelectric coefficients (d_{33} and d_{31}) for that volume were reduced by a factor 1×10^{9}. This alteration of piezoelectric constants effectively modelled the suppressed induced field which characterises closed circuit electrical boundary conditions while maintaining solution accuracy.

C. Comparison of model and experimental results

Beam deflection as a function of MFC-1 drive-voltage is shown in Fig. 4a and clearly shows the linear trend predicted by engineering beam theory and observed by other investigators [22, 34]. Predicted finite element values of cantilever deflection had excellent agreement with experimental values to within 2%. It should be noted that for all, except the value for 160V, the error was within measurement uncertainty of ±10 μm. Fig. 4b and Fig. 4c show beam deflection (D_y) as a function of distance from the clamped region of the cantilever with a drive voltage of 400V applied to MFC-1 and MFC-2 under open and closed circuit boundary conditions respectively. FE-predictions of D_y were again accurate to within 2% compared with experimental values for both conditions. Prediction of closed circuit behaviour showed excellent quantitative agreement with experiment, with predicted cantilever gradient (dy/dz) over the range 120 mm $< z <$ 300 mm matching the measured value of $3.8\mu mV^{-1}$ exactly. In addition, beam tip deflection was predicted to within 1% of the measured value of 0.905 mm. Beam tip deflection decreased under open circuit boundary conditions as compared to closed circuit values, with the predicted and observed values (0.873 mm & 0.880 mm respectively) matching to within 1%. However, beam gradient under open circuit boundary conditions was lower in the model by 2.6%, with FE prediction of $3.7\mu mV^{-1}$ as compared to the experimental value of $3.6\mu mV^{-1}$. This difference in closed and open circuit conditions will not be captured by the thermal approximations to piezoelectric actuation [16, 18, 22]. The small discrepancy between the measured and predicted beam deflection under open circuit conditions indicates that the model generates a larger than expected voltage (via the $V = Q/C$ relation) and electric field in MFC-2 due to the beam deflection. This suggests the relative permittivity used may be too low, leading to increased induced field and hence piezoelectric strain within the MFC-2, increasing the cantilevers effective stiffness. Nevertheless, the excellent agreement for closed circuit response indicates that both elastic and piezoelectric matrices are appropriately formulated. The next stage is to combine the MFC model with a bistable laminate to predict cured shape and snap-through voltage.

V. MFC actuated bistable composite laminates

A. Bistable $[0/90]_T$ and $[-30/60]_T$ composite manufacture

Two cross-ply composite laminates were manufactured using Hexcel carbon fibre-epoxy pre-preg material cut and laid-up by hand and cured at 180ºC. A T700/M21 $[0/90]_T$ laminate and a T800/M21 $[-30/60]_T$

laminate measuring 150×150mm were manufactured from 268gsm unidirectional pre-preg material. A Smart Materials 8557-P1 MFC actuator was bonded to the smooth surface of the laminate to create $[-30/60/0_{MFC}]_T$ and $[0/90/0_{MFC}]_T$ laminates. To ensure good adhesion, bond surfaces were roughened with emery paper and then cleaned with isopropyl alcohol before a thin layer of two-part epoxy was applied to both MFC and laminate. The MFC was positioned centrally on the laminate surface with PZT-fibre direction aligned with *y*-axis (Figs. 1 and 5); the active laminate was then placed between two flat aluminium plates under 200N clamping force for 24hrs to allow the epoxy to cure. The two stable states for the $[-30/60/0_{MFC}]_T$ laminate can be seen in Fig.5a and 5b. Stable states for the $[0/90/0_{MFC}]_T$ laminate can be seen in Figs. 1a and 1b.

B. 'Snap-through' actuation voltage measurement

A function generator was used to provide a DC step-input from zero volts up to the desired test voltage to a power amplifier (TREK PZD700 piezo driver). Actuation voltage was maintained for 60s after the step-input to account for the effects of piezoelectric creep [31]. After each test cycle (i.e. snap-through from State A to State B), voltage was reduced to zero and the laminate disconnected from the amplifier. The laminate was manually snapped into each stable state once before being reset to the starting condition and electrically discharged to ensure that no residual charge influenced system characteristics. The lowest snap-through voltage for both laminates was established via binary search in the range 0 - 1500V with 5V increments between test voltages. Laminates rested on a polished steel table to ensure laminate deflection was not impeded by frictional forces.

C. Measurement of cured shape of bistable composites with MFC

The shapes of the two bistable composites, $[0/90/0_{MFC}]_T$ and $[-30/60/0_{MFC}]_T$, were charaterised using standard three-dimensional motion analysis techniques similar to those in Betts et al. [24]. To examine the influence of actuator attachment on overall shape the $[-30/60]_T$ laminate was also characterised prior to actuator attachment. Three digital video camera recorders (Sony DCR-TRV 900E or Sony HC9, Sony Corporation, Japan) operating at 50 fields per second were set up in an umbrella configuration around the experimental area as shown in [24]. The three cameras were positioned to achieve the best possible viewing angle for each laminate. One camera was always positioned much higher than the other two cameras, which were further away sideways from the laminates. This ensured that the cameras were not in the same plane in accordance to recommendations by Nigg et al. [35]. The distances between the centre of lens and the origin of the measurement volume varied from 1.64 to 2.77 m with the height of the cameras ranging from 0.58 to 1.86 m above the measurement surface. A 20×20×10 mm wire frame was first videotaped on the measurement surface for calibration purposes on both camera set ups. The camera

views were restricted to a volume just slightly larger than the calibration frame. After removing the frame, the laminate was positioned within this measurement volume and videotaped simultaneously with all three cameras.

In order to map arbitrary co-ordinates on the surface of the laminates to later create the shape of the laminate, markers were attached on one surface of the laminate. The $[-30/60]_T$ and $[-30/60/0_{MFC}]_T$ laminates had 145 round colour labels of 8 mm diameter attached to it, as in Fig. 5. The size of the markers were reduced for the $[0/90/0_{MFC}]_T$ laminate allowing 279 markers to be put on the surface. The four corner points in each laminate were also used.

The actual mapping of the surface co-ordinates was carried out using PeakMotus motion analysis system (v. 8.5, Vicon, USA) after transferring the calibration and laminate video clips onto the computer. First, the eight corners of the calibration wire frame were manually digitised from each camera view (and for each camera set up). Then, the centre of each surface marker and the four corners of the each laminate were manually digitised from all three camera views. The digitised area on the computer screen was 1440×1152 pixels. The digitised pixel information from each camera view was combined with the calibration information to transform these to Cartesian co-ordinates of the laminate surfaces using Direct Linear Transformation method [36]. The largest directional co-ordinate RMS error of different set ups between the known eight calibration co-ordinates and the respective digitised point was 0.3 mm. The interpolated surface was then constructed from the raw coordinates using the spline based interpolation method [37] for comparison with FE predictions.

D. Development of MFC actuated bistable composite model

A non-linear large deflection finite element analysis was conducted to predict both cured shape and snap-through voltage. Model convergence was controlled using the line search convergence control method to improve numerical stability [33, 38]. Formulation of this MFC-bistable composite model was far more complex than the simple isotropic aluminium cantilever beam as it is necessary to capture:

(i) The bistable states of the unsymmetrical composite and the corresponding laminate curvature as a result of cooling the unsymmetrical composite from the cure temperature,

(ii) The influence of attaching the MFC actuator to the laminate at room temperature on the curvature of the bistable laminate – MFC combination,

(iii) The prediction of a snap-through event as a result of the application of a voltage to the MFC.

The $[-30/60/0_{MFC}]_T$ laminate was modelled using 20-node quadratic SOLID186 layered brick elements. The laminate was modelled as three volumes shown in Fig 6. A central strip measuring 57×150 mm was located underneath the MFC volume (point 1 in Fig. 6) and was meshed with 1360 elements while the two remaining volumes both measuring 46.5×150 mm (points 2 and 3 in Fig. 6) were meshed with 816 elements each to create the mesh shown in Fig.6a. Maximum element aspect ratio within the laminate was 9.14. All coincident nodes within the laminate volume were then merged to ensure stress transfer during model solution. To make use of symmetry in the $[0/90/0_{MFC}]_T$ laminate, a symmetric boundary condition was imposed along the x = 0mm plane. The mean ply-thicknesses for the laminates with ply angles of $[\theta/\theta+90]_T$ were determined by optical microscopy and used to approximate the laminates individual ply thicknesses. Table 3 shows the mean and standard deviation of ply thickness and total laminate thickness for a range of manufactured laminates with ply angles of $[\theta/\theta+90]_T$. Materials properties for the laminate were determined by batch testing undertaken by Airbus UK [39] for both T700/M21 and T800/M21 pre-preg material and are shown in table 4.

A volume measuring 85×57×0.3 mm was defined and ascribed the homogenised MFC materials properties (Section III) to represent the active area of the Smart Materials MFC8557P1 actuator. The actuator volume was located centrally on the upper surface of the laminate with MFC-fibre orientation aligned with the y-axis as indicated in Fig. 6b. This volume was meshed with 1200 SOLID226 elements with a maximum element aspect ratio of 9.33. With all volumes meshed, coincident nodes on adjacent surfaces of laminate and MFC were merged along with coincident areas to ensure stress transfer between the laminate and MFC volumes. Due to the selection of higher order solid elements it is possible to accurately model bending deformation without multiple elements through the thickness [40] and hence a single element thickness was used. With all volumes meshed and the MFC and laminate volumes merged, the laminate models were mechanically constrained from translation in all three orthogonal directions at the origin of the global coordinate system, shown in Fig. 7. Additionally the node at the point (0, 0, 0.515) was constrained from in-plane translation to ensure the laminate did not rotate about either the x or y-axis (Fig. 7). Due to actuator orientation in the experimental sample, the finite element model must converge to stable deformation State B before application of MFC drive-voltage. To force the finite element solution to converge to State B, temporary displacement constraints were applied at locations of minimum State B deflection as indicated in Fig. 7b.

E. Active laminate model – Model solution

With the model mechanically constrained, the cool down of the bistable composite laminate from the autoclave temperature (180ºC) and attachment of the MFC actuator at room temperature was modelled in a four step process:

(i) A temperature change of -160K was applied to composite elements to ensure laminate converges to State B

(ii) Application of an offset voltage to compensate for thermal stress imposed on MFC volume

(iii) Removal of temporary displacement constraints (shown in Fig. 7b)

(iv) Application of MFC drive-voltage until snap-through of the structure into State A.

Fig. 8a shows the laminate and MFC model at the cure temperature of 180°C which is initially flat. Fig. 8b shows the highly curved structure at a temperature of 20°C with the temporary displacement constraints still in place. Fig. 8b represents stage (i) of the solution process detailed above. Fig. 8c shows the laminate model after application of the offset voltage (V_0) and removal of the temporary displacement constraints, this represents stages (ii) and (iii) of the solution process. During application of MFC drive voltage (stage (iv) in the solution process) the laminate flattened as MFC drive-voltage and the resulting actuation strain increased before undergoing the sudden transition into deformation State A (snap-through).

To model the cool down from elevated curing temperature of the composite laminate a temperature difference was applied to the composite elements. The temperature constraint was applied only to composite (SOLID186) elements while the coupled field (SOLID226) elements of the MFC were not subjected to the imposed temperature constraint since the MFC is attached at room temperature. The electrical degree of freedom for the SOLID226 elements was coupled for nodes of equal *z*-coordinate at 5 mm intervals along the *y*-axis. This constraint ensures that applied field remains well aligned with the poling direction of the MFC model and minimise variation in the field along the y-axis of the MFC volume. During model development it was noted that solutions of bistable laminates with the MFC model integrated exhibited significantly reduced curvature and did not exhibit a second stable configuration but rather always adopted the State A configuration after application of the thermal load step. This phenomenon was attributed to the interaction of the MFC and laminate under the action of the imposed thermal load at stage (i). Although the composite elements were subjected to the imposed thermal load, the MFC elements experienced an elastic strain comprising the thermal strain of the composite and the mechanical strain caused by laminate deformation deforming the MFC volume. As nodes within the MFC volume are merged with those on the laminate surface before the temperature change is imposed, both mechanical and thermal strains were imposed upon the MFC model. This introduces an additional mechanical stress within the MFC volume which does not represent the true experimental conditions. To compensate for the superposed thermal stress an 'offset voltage' was applied to the MFC. Via the

converse piezoelectric effect the offset voltage created a stress field of equal magnitude but of opposite sign to that created by the imposed thermal strain. The total thermal strain in the portion of laminate bonded to the MFC was calculated by considering the MFC as an elastic constraint resisting the thermal contraction. The strain in both laminate and MFC due to thermal contraction of the composite laminate must be equal, hence force equilibrium leads to:

$$\varepsilon_M = \frac{\varepsilon_T K_1}{K_1 + K_2} \qquad \text{(Eqn 8)}$$

where ε_M is the observed strain within the MFC, ε_T and K_1 are the unconstrained thermal contraction and transformed reduced stiffness of the layer to which the MFC is bonded while K_2 is the MFC stiffness; all properties are measured in the *y*-direction and are aligned with MFC-fibre orientation. The transformed reduced stiffness may be calculated from the orthotropic elastic constants of each layer using [29]:

$$\overline{Q_y} = Q_{11}\cos^4\theta + 2(Q_{12} + 2Q_{66})\sin^2\theta\cos^2\theta + Q_{22}\sin^4\theta \qquad \text{(Eqn 9)}$$

where $\overline{Q}_y$ is the transformed reduced stiffness in the *y*-direction of the global coordinate system, Q_{ij} is the reduced stiffness values measured in the material coordinate system and θ the orientation of the material coordinate system with respect to the global coordinate system. In this case the global coordinate system whose first principal direction is the *y*-direction as shown in Fig 9a.

The offset voltage required to compensate for the imposed thermal strain may be calculated using:

$$V_O = \varepsilon_M S_E \Big/ d_{33} \qquad \text{(Eqn. 10)}$$

where V_0 is the offset voltage, ε_M the observed strain in the MFC and S_E is the electrode separation in the FE model. The volt degree of freedom for nodes on the y = 42.5 mm face of the MFC model (indicated in Fig. 9b) were coupled and forced to the offset voltage value while nodes on the y = -42.5 mm face were constrained to zero volts. This created an effective electrode separation of 85 mm in the FE model.

Piezoelectric actuation was modelled by applying a voltage constraint (V_c) on nodes at y = 42.5 mm to create a change in the electric field in the MFC. The voltage constraint was applied as a ramp change from the offset voltage (V_0), with several intermediate time steps specified between V_0 and V_c to ensure that the model followed the load path accurately. As specified for non-linear buckling analysis in situations where the arc-length method is not appropriate [26], snap-through was identified as the lowest value of voltage constraint at which the no longer model converged to State B (i.e. snap-through into State A had occurred).

F. Laminate shape (model and experimental)

Predicted shape of a $[-30/60/0_{MFC}]_T$ active laminate in State B is shown in Fig 10a with deviations from simple cylindrical curvature seen at points A and C. The meshed regions in Fig 10a are the FE predictions and the solid coloured sections are the experimental measurement. Overall the agreement between the two is very good. The laminate adopts a saddle-shape after MFC addition with a significantly flattened section directly underneath the MFC (point B). This reduction in curvature underneath the MFC indicates that the bending stiffness of the actuator has a significant effect on the cured shape of the laminate. When comparing maximum deflections with respect to the laminate geometric centre (D_{max}) before and after MFC-bonding, the influence of MFC addition is clear with measured deflections of 38.2 mm for the laminate (without MFC) and reducing to 22.5 mm after MFC addition. Maximum deflection for the $[-30/60/0_{MFC}]_T$ laminate after MFC addition was predicted to be 25.20 mm for State B, 12.1% higher than the measured maximum deflection of 22.48 mm.

Figure 10b shows interpolated surface plot of experimental measurement of laminate deflection for the $[0/90/0_{MFC}]_T$ laminate in State B with the FE predicted overlaid as a mesh. The results again show close agreement between model and experiment. Maximum deflection for the $[0/90/0_{MFC}]_T$ laminate after MFC addition was predicted to be 10.73 mm for State B, 16% lower than experimentally measured maximum deflection of 12.77 mm. Variations in laminate composition and ply orientation commonly seen during hand manufacture can create variations in observed laminate deflection [24]. Due to the high sensitivity of predicted deflection to laminate composition, it is likely that small deviations from the mean MFC thickness and PZT volume fraction would also introduce errors. The combined effect of these unknown variations in laminate and MFC composition could account for the observed errors in predictions of laminate deflection. Despite limitations in quantitative prediction the model captures the cured shape and local reversals of curvature very well.

G. Snap-through (model and experiment)

Finite element prediction of snap-through voltage was achieved for both laminates, with non-linear buckling analyses predicting behaviour prior to snap-through. For the $[0/90/0_{MFC}]_T$ laminate the model predicts snap-through at 645V while experimental observation showed that a drive voltage of 670V induced snap-through. In the case of the $[-30/60/0_{MFC}]_T$ laminate the predicted and observed snap-through voltages were 677V and 700V, respectively. The predicted snap-through voltages are in excellent agreement with the measured values with errors compared to experiment of less than 4.5% in both cases. Delayed snap-through was observed at voltages immediately below monotonic snap-through voltage when drive-voltage applied for a prolonged time period. This was due to creep of the MFC actuators [31] and

could be compensated for in industrial applications using time varying input signals [32] and closed-loop control. Due to the discontinuity of the voltage-deflection curve associated with snap-through the Newton-Raphson solution procedure was not able to predict laminate response throughout the entire load cycle even with line search convergence control enabled.

In order to fully track voltage-deflection behaviour of bistable laminates under MFC actuation implementation of non-linear stabilisation or the arc-length solution methods is necessary. However neither non-linear stabilisation nor the arc-length solution methods are currently implementable with SOLID226 elements. Therefore the presented model represents the most appropriate formulation within the ANSYS V11.0 finite element software and has significantly extended modelling capability and accuracy of coupled field finite element models in the prediction of actuation behaviour of bistable composites.

VI. Conclusions

A homogenised finite element model of a commercially available MFC actuator has been developed and validated to allow prediction of actuator performance under combined electrical and stress fields. Three dimensional piezoelectric and stiffness matrices for the MFC were calculated using experimentally determined orthotropic constants to create a homogenised material model of the MFC actuator. This data was validated by comparing finite element predictions to experimental measurements of tip deflection of an isotropic beam with MFC actuators bonded to both top and bottom surfaces. Predicted values of deflection agreed with experiment to within 2.5% over this range. With an MFC under closed circuit boundary conditions both deflection and gradient of the beam were predicted to within 1% of experimental measurement. Under open circuit conditions, the developed electrical field within the MFC caused a reduction in beam gradient remained within 1% of experimental values.

The MFC model was integrated with the model for bistable laminates to predict cured shape and snap-through behaviour of two cross-ply bistable laminates. Challenges associated with integration of coupled field elements with the composite structure have been addressed through application of an offset voltage to compensate for undesired thermal stresses within the MFC volume. Prediction of cured shape after MFC addition is in good agreement with experimental measurement with maximum error between prediction and measured values of 12-16%. The change in cured shape caused by MFC addition and localised variation in curvature were predicted, and quantitative prediction of laminate deflection agrees with experiment sufficiently to aid prototype design. Snap-through voltage for both $[0/90/0_{MFC}]_T$ and [-

$30/60/0_{MFC}]_T$ laminates were predicted to within 4.5% of experimental measurements which is a significant improvement upon previously unvalidated attempts at predicting snap-through. By including correctly formulated homogenised MFC properties as well as appropriate electrical constraints the presented model improves and extends the applicability of finite element techniques available for mechanism design of morphing structures based on bistable composites.

Acknowledgements.

We wish to acknowledge support of Great Western Research (GWR) and Airbus.

References

[1] S. Barbarino, S. Ameduri, L. Lecce, A. Concilio, "Wing Shape Control through an SMA-Based Device", J. Int. Mat. Sys. Struct., vol. 20, pp. 283-296, 2009.

[2] A. Natarajan, R.K. Kapania, D.J. Inman, "Aeroelastic optimization of adaptive bumps for yaw control", J. Aircraft., vol. 4, pp. 175-185, 2004.

[3] M.R. Schultz, "A concept for airfoil-like active bistable twisting structures", J. Int. Mat. Sys. Struct., vol. 19, pp. 157-169, 2008.

[4] C.R. Bowen, R. Butler, R. Jervis, H.A. Kim, A.I.T. Salo, "Morphing and shape control using unsymmetrical composites", J. Int. Mat. Sys. Struct., vol. 18, pp. 89-98, 2007.

[5] M.W. Hyer, "Calculations of the room-temperature shapes of unsymmetric laminates", J. Comp. Mat., vol. 15, pp. 296-310, 1981.

[6] P.F. Giddings, C.R. Bowen, A.I.T. Salo, H.A. Kim, "Bistable composite laminates: Effects of laminate composition on cured shape and response to thermal load", Comp. Struct., vol. 92, pp. 2220-2225, 2010.

[7] C.R. Bowen, R. Stevens, L. J. Nelson, A. C. Dent, G. Dolman, B. Su, T.W. Button, M.G. Cain and M. Stewart, "Manufacture and characterization of high activity piezoelectric fibres", Smart Materials and Structures, vol. 15, pp. 295–301, 2006

[8] B. Jaffe, W.R Cook, "Piezoelectric ceramics." Academic Press, London, 1971, UK. ISBN: 1-878-907170-3

[9] B.R. Williams, D.J. Inman and W.K. Wilkie, "Nonlinear Response of the Macro Fiber Composite Actuator to Monotonically Increasing Excitation Voltage." J Int Mat Sys Struct, vol. 17, pp. 601 – 608, 2006.

[10] R. Paradies and B. Schlapfer, "Finite element modeling of piezoelectric elements with complex electrode configuration." Smart Materials & Structures, 18 (2). 025015, 2009.

[11] C.R. Bowen, A. Bowles, S. Drake, N. Johnson and S. Mahon, S. "Fabrication and finite element modelling of interdigitated electrodes." Ferroelectrics, vol. 228, pp. 257-269, 1999.

[12] J.M. Lloyd, R.B. Williams, D.J. Inman, and W.K. Wilkie, "An analytical model of the mechanical properties of the Single Crystal Macro-Fiber Composite actuator." SPIE Proc., Society of Photo-Optical Instrumentation Engineers, Bellingham, vol. 6(2), pp. 37-46, 2004.

[13] A. Deraemaeker, H. Nasser, A. Benjeddou, and A. Preumont, "Mixing Rules for the Piezoelectric Properties of Macro Fiber Composites." Journal of Intelligent Material Systems and Structures, vol. 20, pp. 1475-1482, 2009.

[14] C.R. Bowen, L.J. Nelson, R. Stevens, M.G. Cain and M. Stewart,"Optimisation of interdigitated electrodes for piezoelectric actuators and active fibre composites." Journal of Electroceramics, vol. 16, pp. 263-269, 2006.

[15] S.C. Choi, J.S. Park and J.H. Kim, "Vibration control of pre-twisted rotating composite thin-walled beams with piezoelectric fiber composites." Journal of Sound and Vibration, vol. 300, pp. 176-196, 2007.

[16] P. Portela, P. Camanho, P. Weaver and I. Bond, "Analysis of morphing, multi stable structures actuated by piezoelectric patches." Computers & Structures, vol. 86, pp. 347-356, 2008.

[17] P. Binette, M.L. Dano and G. Gendron, "Active shape control of composite structures under thermal loading." Smart Materials & Structures, vol. 18, 025007, 2009

[18] M.R. Schultz and M.W. Hyer, "Snap-through of unsymmetric cross-ply laminates using piezoceramic actuators." Journal of Intelligent Material Systems and Structures, vol. 14, pp. 795-814, 2003.

[19] T. Ikeda, "Fundamentals of Piezoelectricity." Oxford University Press, Oxford, UK, 1990 ISBN: 0-198-56339-6

[20] H. Jaffe and D.A Berlincourt, "Piezoelectric transducer materials." Proceedings of the IEEE, vol. 3, pp. 1372-1386, 1965.

[21] M.L Dano, M. Gakwaya and B. Julliere, "Compensation of thermally induced distortion in composite structures using macro-fiber composites." Journal of Intelligent Material Systems and Structures, vol. 19, pp. 225-233, 2008.

[22] L.B. Ren, "A theoretical study on shape control of arbitrary lay-up laminates using piezoelectric actuators." Composite Structures, vol. 83, pp. 110-118, 2008

[23] J. Etches, K. Potter, P. Weaver, and I. Bond, "Environmental effects on thermally induced multistability in unsymmetric composite laminates.", Composites Part A-Applied Science and Manufacturing, vol. 40, pp. 1240-1247, 2009.

[24] D.N. Betts, A.I.T Salo, C.R. Bowen and H.A. Kim, "Characterisation and modelling of the cured shapes of arbitrary layup bistable composite laminates." Composite Structures, vol. 92, pp. 1694-1700, 2010.

[25] M. Gude and W. Hufenbach, "Design of novel morphing structures based on bistable composites with piezoceramic actuators." Mechanics of Composite Materials, vol. 42, pp. 339-346, 2006.

[26] ANSYS Inc . 2007. Structures with Geometric non-linearities. Paper 3. Ansys Theory Reference V11.0.

[27] M. Gude, W. Hufenbach, C. Kirvel, Piezoelectrically driven morphing structures based on bistable unsymmetric laminates, Composite Structures, vol. 93, pp. 377–382, 2011.

[28] R.B Williams, D.J. Inman, M.R. Schultz, M.W. Hyer and W.K. Wilkie, "Nonlinear tensile and shear behavior of macro fiber composite actuators." Journal of Composite Materials, vol. 38, pp. 855-869, 2004.

[29] M.W. Hyer, "Stress Analysis of Fibre Reinforced Composite Materials." WCB/McGrawhill, Boston, Mass., 1998, ISBN: 0-071-15983-5

[30] "MFC Brochure 2010 V3."(2010). http://www.smart-material.com/media/Publications/MFC-brochure_2010_V3.1.pdf Accessed: Dec 15, 2010.

[31] H. Jung and D.G. Gweon, "Creep characteristics of piezoelectric actuators." Review of Scientific Instruments, vol. 71, pp. 1896-1900, 2000.

[32] H. Jung, J.Y. Shim and D.G. Gweon, "Tracking control of piezoelectric actuators." Nanotechnology, vol. 12, pp. 14-20, 2001.

[33] ANSYS Inc . 2007. Coupled field analysis guide. Ansys user help reference system V11.0.

[34] P.Giddings, C.R.Bowen, H.Kim and R.Butler, "Characterisation of actuation properties of piezoelectric bi-stable carbon-fibre laminates", Composites Part A, vol. 39, pp. 697-703, 2008.

[35] B.M. Nigg, G.K. Cole and I.C. Wright, Optical methods. In: Nigg, B.M., Herzog, W. (eds.). Biomechanics of the musculo-skeletal system. Chichester, UK: John Wiley & Sons. pp. 362–391, 2007.

[36] Y.I. Abdel-Aziz and H.M. Karara, "Direct linear transformation from comparator coordinates into object space coordinates in close-range photogrammetry". In: Proceedings of the ASP/IU symposium on close-range photogrammetry. pp. 1–118, 1971.

[37] D.T. Sandwell, "Biharmonic Spline Interpolation of Geos-3 and Seasat Altimeter Data." Geophysical Research Letters, vol. 14, pp. 139-142, 1987.

[38] ANSYS Inc . 2007. Newton-Raphson Procedure. Paper 15. Ansys Theory Reference V11.0

[39] M. Desailloud,"Modulus harmonisation of HS & IM tape composite materials." *Rep. No. ESAC_RP0306315*, Airbus Section 530, 2004.

[40] ANSYS Inc . 2007. Structures with Geometric non-linearities. Paper 3. Ansys Theory Reference V11.0

Table 1: Mechanical properties of Smart Materials Corp M8557-P1 MFC actuator taken from Williams *et al*. [28] and manufacturers data sheet [30].

	Williams *et al* 2004.	Smart Materials Corp.
E_{33} (*GPa*)	29.4	30.336
E_{11} (*GPa*)	15.2	15.857
G_{31} (*GPa*)	6.06	5.515
Y_{31}	0.312	0.31
Y_{13}	0.16	0.16

Table 2: Piezoelectric coupling coefficients [d_{ij}] and relative permittivity (ε_i) of Smart Materials M8557 MFC actuator. Note ANSYS used permittivity at constant strain and an input parameter [ε^s_{ij}].

	Smart Materials Corp M8557-P1 MFC actuator
d_{33} (pm/V)	467
d_{32} (pm/V)	-210
d_{31} (pm/V)	-210
ε^s_{11}	712
ε^s_{22}	1.7
ε^s_{33}	737

Table 3: Mean and standard deviation (σ) of ply and total laminate thickness for $[\theta/\theta+90]_T$ laminates made from 268gsm M21/T800.

	Idealised	Measured	
	Thickness (mm)	Thickness (mm)	σ
θ˚ ply	0.25	0.255	0.013
θ +90˚ ply	0.25	0.233	0.018
Resin layer	0	0.027	0.021
Total	0.5	0.515	0.045

Table 4: Elastic properties of 268gsm-1 T800/M21 material and T700/M21 * indicates values calculated using stress-strain relations described in [29].

Property [*unit*]	T700/M21	T800/M21
E_1 [GPa]	148	172
E_2 & E_3 [GPa]	7.8	8.9
G_{12} & G_{23} [GPa]	3.8	4.2
G_{23}* [GPa]	0.02	0.02
ν_{12} & ν_{13}	0.35	0.35
ν_{23}*	0.01	0.01
α_1 [1×10^{-7} $^oC^{-1}$]	-0.9	-0.9
α_2 & α_3 [1×10^{-5} $^oC^{-1}$]	3	3
E_r [GPa]	1.5	1.5
ν_r	0.4	0.4
α_r [1×10^{-5} $^oC^{-1}$]	9	9
Density [kgm^{-3}]	1072	1072

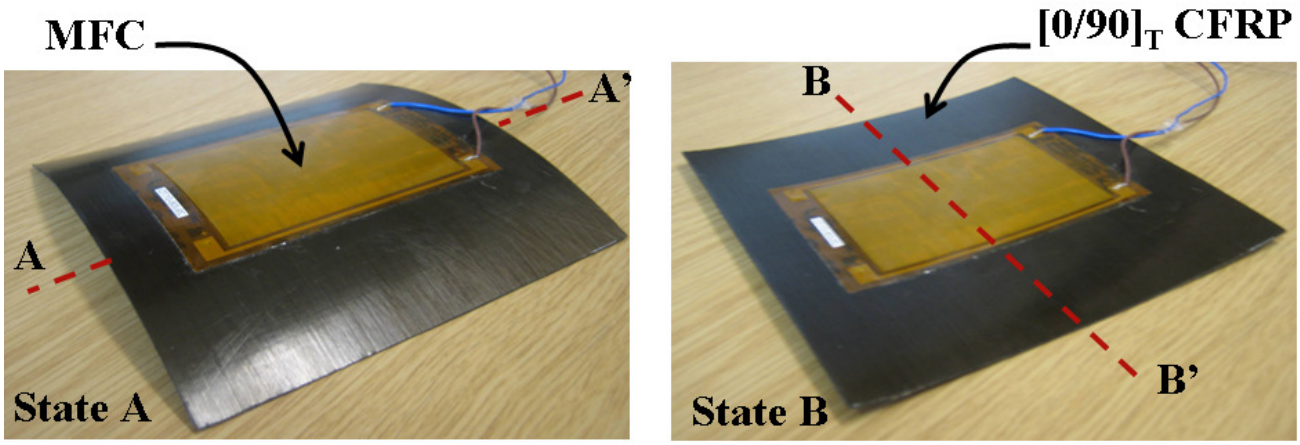

(a) (b)

Fig. 1. $[0/90/0_{MFC}]_T$ laminate in State A (a) and State B (b) with axis of curvature shown as dashed line.

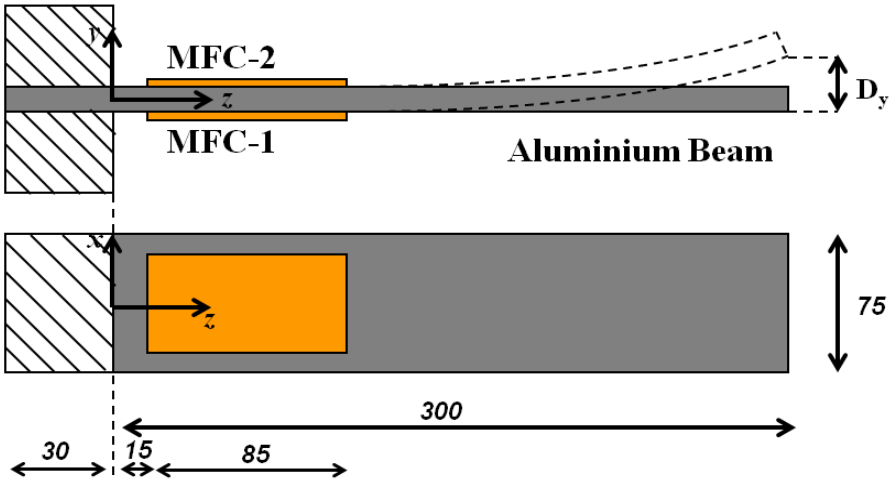

Fig. 2: Experimental setup with aluminium beam, driven actuator (MFC-1) and passive actuator (MFC-2) with dimensions shown in *mm*.

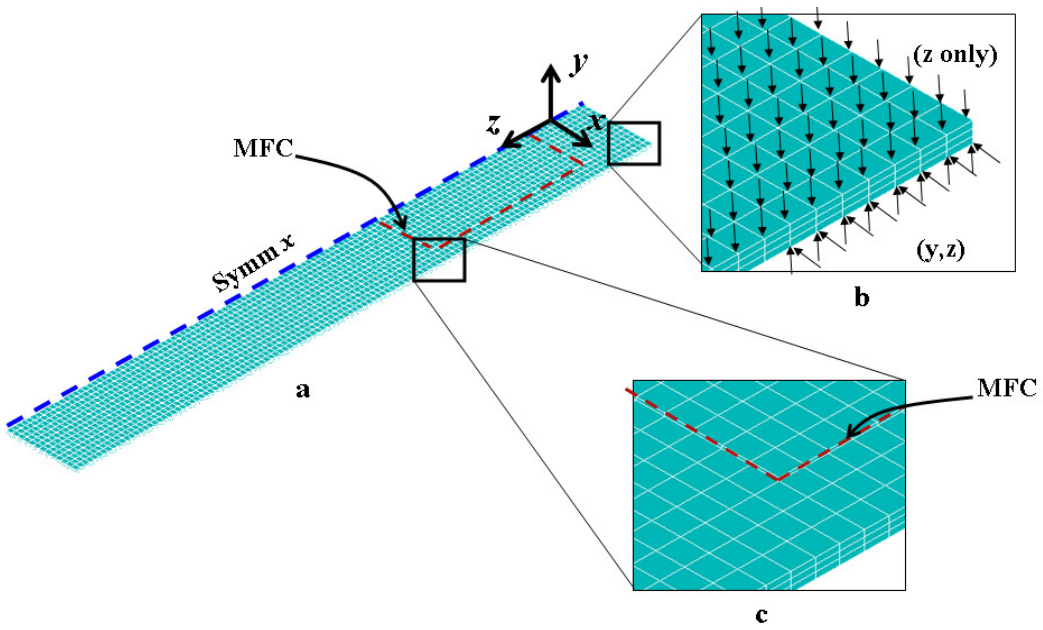

Fig. 3: Finite element model used to predict beam deflection showing coordinate system and symmetric boundary constraint (a), mechanical constraint to model clamped end condition of experimental set up and mesh density of both MFC volume and beam (c).

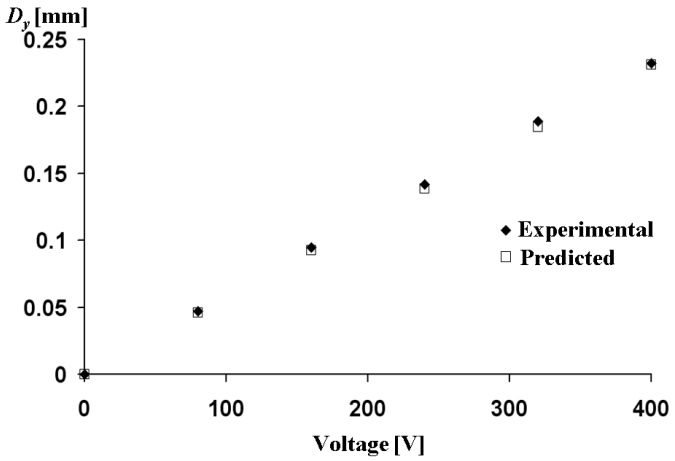
D_y [mm]
0.25
0.2
0.15
0.1
0.05
0
0
100
200
300
400
Voltage [V]
Experimental
Predicted

(a)

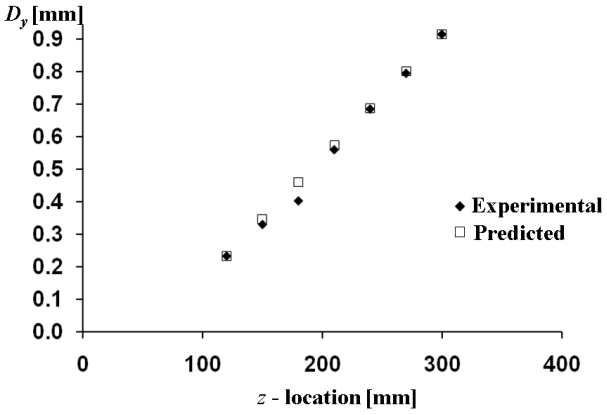
D_y [mm]
0.9
0.8
0.7
0.6
0.5
0.4
0.3
0.2
0.1
0.0
0
100
200
300
400
z - location [mm]
Experimental
Predicted

(b)

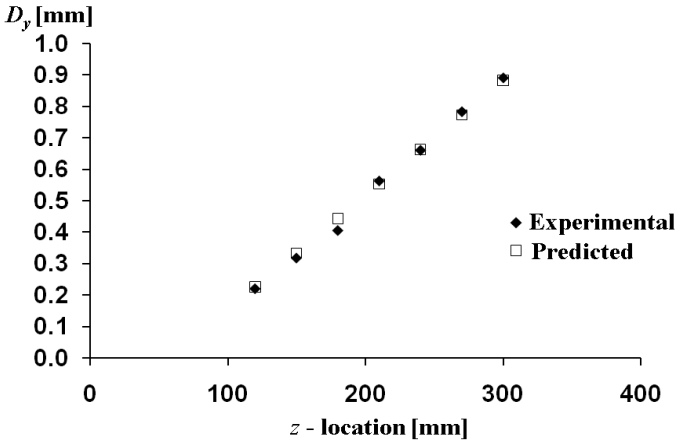

(c)

Fig. 4 (a) Beam deflection (D_y) as a function of MFC drive-voltage. (b) D_y as a function of z-location with MFC-2 under open circuit boundary conditions. (c) D_y as a function of z-location with MFC-2 under closed circuit boundary conditions.

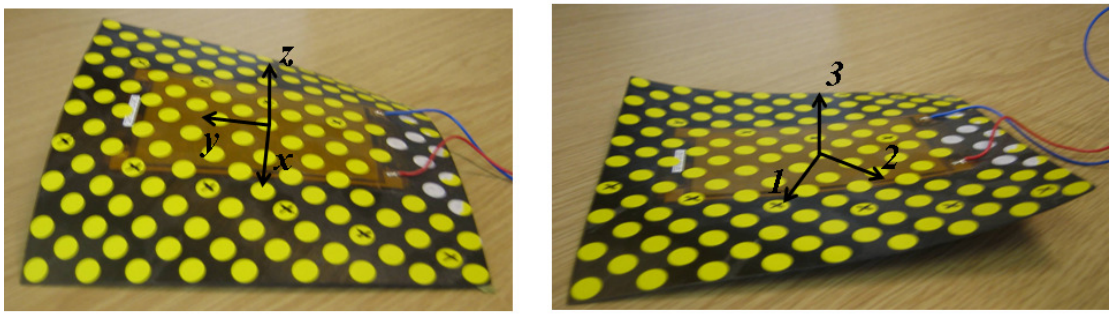

a *b*

Fig. 5: Cured shape of [-30/60/0$_{MFC}$]$_T$ laminate in State A (a) with global coordinate system (*a*) and State B showing local material coordinate system for uppermost 60˚ ply (*b*). Circular markers are attached for co-ordinate mapping of the surface.

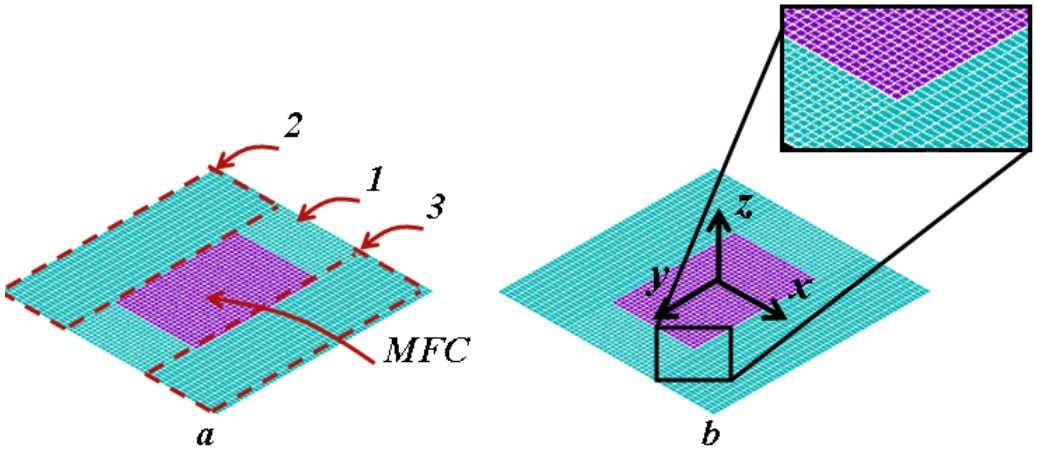

Fig. 6: Meshed finite element model of $[-30/60/0_{MFC}]_T$ laminate showing three laminate volumes (1, 2 and 3) and centrally located MFC volume (a) overall mesh density and detail of coincident nodes near corner of MFC volume and global coordinate system (b).

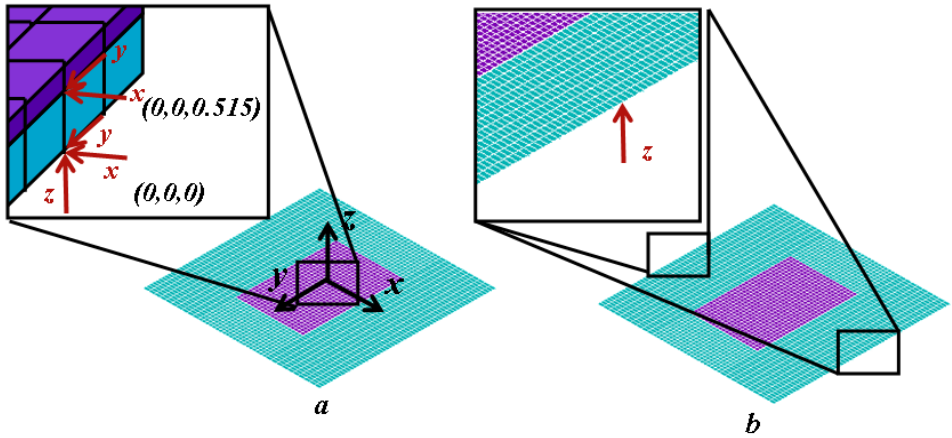

Fig.7: Meshed finite element showing mechanical constraint at origin of global coordinate system (a) and temporary mechanical constraint used to force model convergence to deformation State B (b).

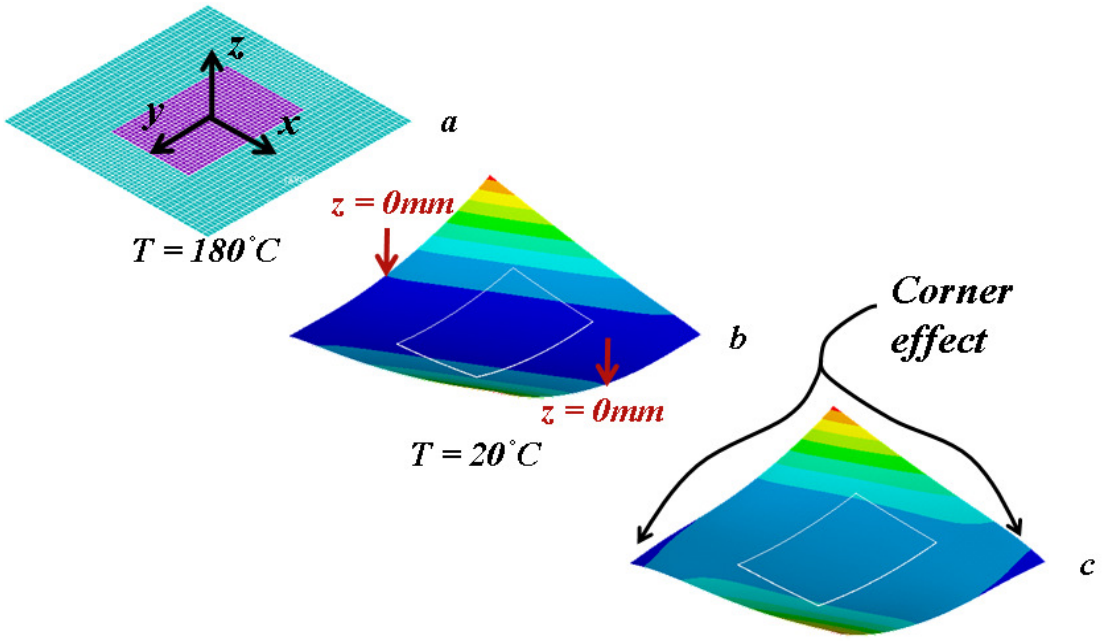

Fig.8: Finite element prediction of cured shape for $[-30/60/0_{MFC}]_T$ laminate at cure temperature of 180°C (a) room temperature of 20°C (b) and in stable deformation State B with offset voltage (V_0) applied (c).

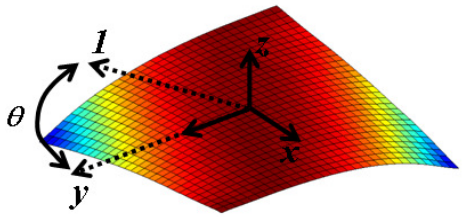

(a)

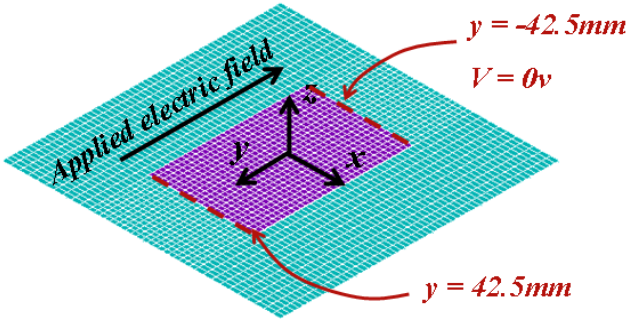

(b)

Fig. 9: (a) $[-30/60/0_{MFC}]_T$ laminate showing orientation material coordinate system of the uppermost 60˚ layer, showing angle θ between the *1*-direction of the local system and *y*-direction of the global system. (b) Finite element model of $[-30/60/0_{MFC}]_T$ laminate showing electrical constraint at y = -42.5mm and location of drive-voltage application at y = 42.5mm and the resulting direction of applied electric field.

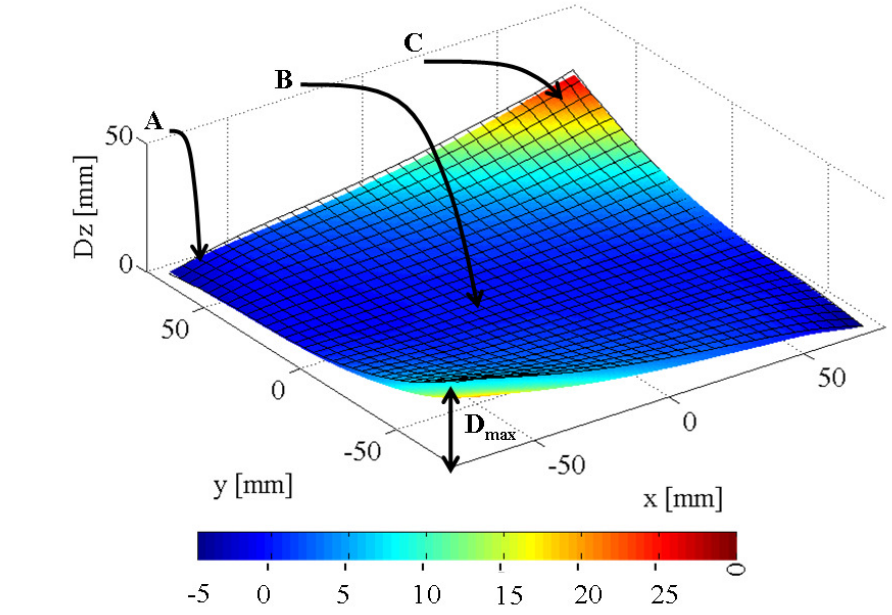

(a)

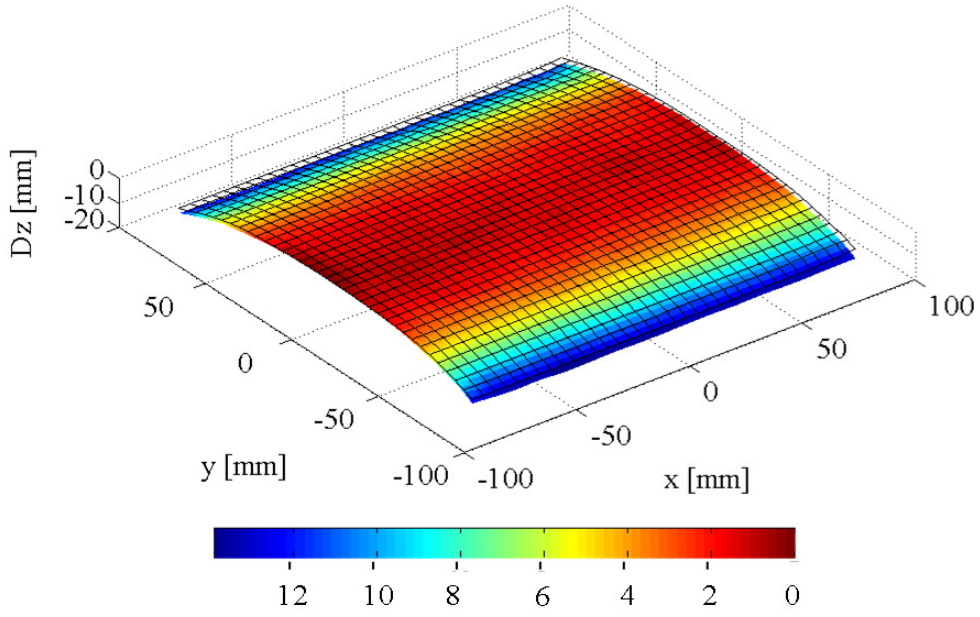

(b)

Fig.10 (a) Interpolated surface plot of 149 measured surface coordinates showing the [-30/60/0$_{MFC}$]$_T$ laminate in State B with FE-predicted surface overlaid as mesh. (b) Interpolated surface plot based on 283 measured surface coordinates showing the [0/90/0$_{MFC}$]$_T$ laminate in State B with FE-predicted surface overlaid as mesh ***(laminate shown inverted for clarity of presentation).***